The role of stellar flares in planetary transits and exoatmospheres

Author: Robert Vila Alsina
Facultat de Física, Universitat de Barcelona, Diagonal 645, 08028 Barcelona, Spain. *

Advisor: Octavi Fors Aldrich
Dept. de Física Quàntica i Astrofísica, Institut de Ciències del Cosmos (ICCUB), Universitat de Barcelona, IEEC-UB, Martí i Franquès 1, E-08028 Barcelona, Spain.

Abstract: As the methods to characterize exoatmospheric components improve, the role played by stellar activity in the transmitted spectra is enhanced. Accurately detecting and modeling contributions like stellar flares is essential to remove their signals from the spectra. In this work, we analyze the light curves of TRAPPIST-1 b for the transits observed by the JWST NIRISS on 18 and 20 Jul 2022. A stellar flare during the transit has been found for 20 Jul using MCMC fitting and checking H_α emission. Our results indicate that, if not properly modeled and erased, flare contribution can mask and be misinterpreted as an atmospheric signal. The event found also has chemical implications, as the UV radiation emitted can induce certain chemical reactions. Furthermore, depending on its characteristics, it can be fatal for complex living organisms. This study highlights the importance of accounting for stellar activity in exoplanet studies to avoid misdetections and better understand the star-planet interaction.

I. INTRODUCTION

With the James Webb Space Telescope (JWST) out in space, exoplanet science is taking a giant leap forward: we can finally characterize some components of exoatmospheres. This achievement can be completed by focusing the telescope on the star during a predicted transit, taking a series of spectroscopic data as the planet passes in front of the star. As expected, the footprint of the chemical elements requires unprecedented precision. Using the explained technique, some groups have already detected evidence of potential biomarkers presence in exoplanets [1].

One of the main targets for exoatmospheric observations with JWST are planets orbiting M-dwarf stars. M-dwarf stars show a high activity level such as flares, starspots, and faculae. This stellar activity is meant to strongly interact with biological activity, giving the necessary energy for some biochemical reactions to occur; or destroying them with strong or frequent radiation. Furthermore, super-Earth-sized ($m = 1 - 10\mathbf{M}_\oplus$) rocky planets have been found to be very frequently orbiting M-dwarf stars [2].

A stellar flare is an explosive phenomenon produced by magnetic reconnection that heats the plasma due to electron acceleration following field lines. As the characteristic spectra of this phenomenon are not the same as the ones from the host star in quiescent mode, new tools and models have to be developed to detect and subtract the signal from the activity. An approximation to fit a flare spectra can be a black body with some overlapped emission lines. This black-body spectrum evolves with time as the temperature decreases from an initial effective value of 9,000K-16,000K.

One example of these stellar systems with an active M-type host star, already observed by JWST, is TRAPPIST-1. The interest behind this target is the presence of seven transiting planets orbiting an M8-type dwarf star, three of them Earth-like orbiting in the habitable zone (HZ) of the system [3]. The small size of the host star makes the relative contributions of the hypothetical atmospheres greater. All these characteristics combined make them one of the most interesting objects to study in-depth, with some similar planets orbiting the same star at different distances.

Nonetheless, some studies evidenced strong stellar contamination in the transmitted spectra which dominates in front of the signal left by the chemical components in the transmitted signal [4, 5].

In this work, we will study the effect of stellar activity in the different wavelengths of a transmitted spectrum of two exoplanet transits. These transits are both from TRAPPIST-1 b on 18 Jul 2022 and 20 Jul 2022 taken with Near Infrared Imager and Slitless Spectrograph (NIRISS) by JWST (Proposal GO-2589, PI: O. Lim). The Spectrograph was used as mode Single Object Slitless Spectroscopy (SOSS). A time-series spectroscopy will be analyzed from uncalibrated JWST data. Using `exoTEDRF`[1] [6] pipeline, a time-flux curve will be obtained to fit different models with `Allesfitter`[2] [7]. A stellar flare model will be compared with a starspot one to determine which leads to less residual noise when fitted to the time-flux curve.

In Section II a summary of the methodology used to perform the calibrations and the fits is presented. The light curves and their transits and stellar activity are discussed in Section III. The conclusions of the research are

*Electronic address: rvilaalsina@outlook.com

[1] `https://github.com/radicamc/exoTEDRF`
[2] `https://github.com/MNGuenther/allesfitter`

in section IV.

II. METHODOLOGY

A. Data calibration

Python package `exoTEDRF`, (formerly `supreme-SPOON`) goes through four stages to obtain precise time-flux-wavelength spectroscopy from JWST uncalibrated data. *Stage 1* performs detector level calibrations. The software detects and subtracts pixel over-saturation, $1/f$ readout noise, and background model for NIRISS and corrects more non-linearities. *Stage 2* targets further, high-level spectroscopic calibrations. *Stage 3* constructs and fits a model for the slit light trace to finally obtain the 1-D spectral extraction for every time step and each order. *Stage 4* works directly over the 1-D spectrum to correct further contaminants.

We followed all the calibration described in *Stage 1* until the last step, `RampFitStep`. At this point, the code is programmed to compute the mean count rate for every pixel. However, due to our limited computational resources and the high cost required, it was not possible to pursue this pipeline. The source of this problem is the high accuracy of the JWST images and the large size of each file that this involves. The time component is also multiplying the procedure by 155 integrations.

To keep further on our scientific objectives, we contacted the principal investigator of TRAPPIST-1 b JWST proposals, Olivia Lim, and she provided us with the already calibrated spectra. The shared file contains a precise spectrum for each time iteration for both planetary transits as we can see in FIG. 1. These processed spectra were obtained using NIRISS dAta reduction MEthod for exopLanEt SpectroScopy (`NAMELESS`) pipeline. This Python code performs almost the same steps described for `exoTEDRF` and gives very similar and equally useful results.

From the time-series spectra, a simple numerical integration is enough to derive the broadband light curves for every transit. As just the relative flux is needed to fit the different models, this integral can be the sum of every flux point in the desired wavelength range. The transits from different wavelengths will be used to detect certain phenomena with different chromatic shapes than the host star surface. One of these occasions is for stellar flares, where there is a strong H_α emission we can take advantage of [5]. The range that will be considered for the H_α band is 0.652-0.660 μm. Analyzed observations can be accessed here[3].

B. Activity model fitting

The software `Allesfitter` will be used to fit the physical models on the derived stellar time-flux curves. `Allesfitter` is an open-source `Python` package that pro-

[3] `https://doi.org/10.17909/b0ee-8j61`

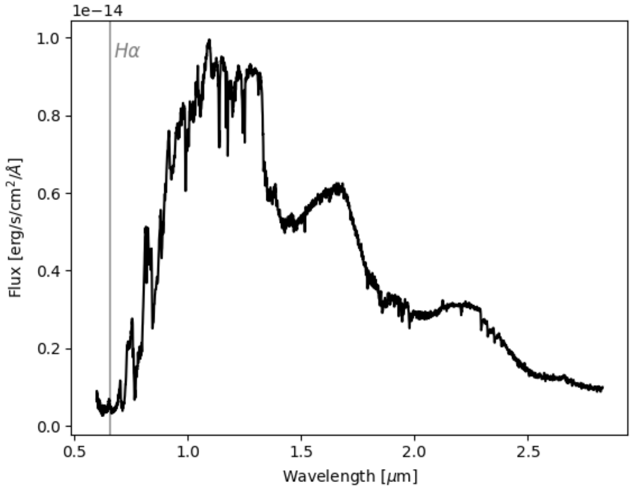

FIG. 1: NIRISS/SOSS spectra of TRAPPIST-1 reduced with `NAMELESS` pipeline. It is an example of the time series spectra of the TRAPPIST-1 b transit in front of the star. The gray vertical line is the interval considered for H_α.

vides a set of tools to fit different models to our data series simultaneously. Some of the models provided that can be of interest are exoplanet transits and stellar activity. In this work we will use Markov-Chain Monte Carlo (MCMC) to fit different parameters of a dependent stellar flux function: an exoplanet transit, a stellar flare, and a starspot. Linear stellar flux variability and limb darkening will also be fitted. For every parameter we want to determine, we have to fix an expected value and a uniform or Gaussian expected range around it.

`Allesfitter` uses the software `ellc` [8] to fit exoplanetary transits. Once given an approximate value of the mid-time transit, orbital parameters, and planet period, the program runs MCMC to find more precise values. After some trials, the number of total steps performed was 3400 for every fit, with 400 walkers. The flux during the transit is computed as numerical Gaussian-Legendre quadrature and analytical expressions for the surface of both overlapping bodies. The same software is used to estimate the flux variation of a starspot. In this case, the input parameters given are the latitude, longitude, brightness, and size of the active region in the host star. They are modeled as integrated triaxial ellipsoids.

Unlike starspots, stellar flares are explosive events in the star's atmosphere due to the magnetic acceleration of ionized plasma. The sharp flux bump they produce differs from other forms of stellar activity. The emission of a stellar flare is mostly in the continuum as a black body. However, there is also an important H_α emission. Therefore we will fit the models to the integrated flux for all the spectrum; or directly in the H_α band. To model this phenomenon, our software considers three parameters: the peak time t_{peak} , amplitude A, and FWHM. First of all, the detected flare is subtracted and normalized from the background stellar flux. This subtracted

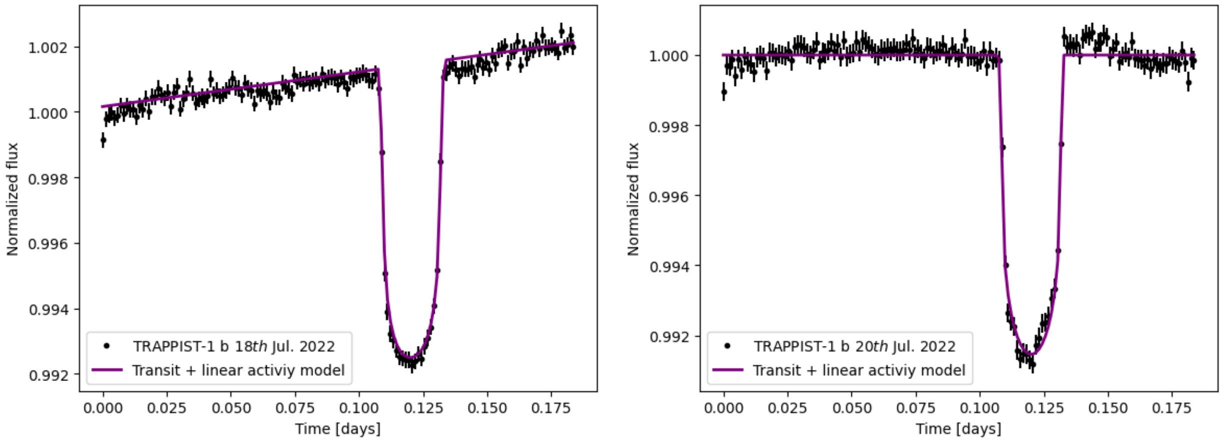

FIG. 2: TRAPPIST-1 normalized flux as a function of time when TRAPPIST-1 b transit occurs. LEFT:18 Jul 2022, RIGHT:20 Jul 2022. In black, the time series of broadband integrated spectra with standard deviation error bars. In purple, the transit model fitted considering linear stellar activity using MCMC with `Allesfitter`.

curve is normalized both in time and amplitude. At this point, we separate in t_{peak} . For the rising behavior, the fitted function is a third-order polynomial:

$$F_{\text{rise}} = 1 + c_1 t_{1/2} + c_2 t_{1/2}^2 + c_3 t_{1/2}^3 + c_4 t_{1/2}^4, \quad (1)$$

and for the decreasing one, the function adjusted is a double-exponential subtraction from the flux normalized to 1:

$$F_{\text{decay}} = 1 + c_1 e^{-c_2 t_{1/2}} + c_3 e^{-c_4 t_{1/2}}. \quad (2)$$

To compare the goodness of different fits, Pearson's χ^2 test will be implemented [9].

III. RESULTS

A. Light curves integration and exoplanet transits

We performed a broadband integration of every spectrum in the time series reduced with `NAMELESS`. Then, the flux was normalized with the global mean of all the points. This process was carried out for both 18 Jul 2022 and 20 Jul 2022 transits. With JWST precision it is possible to detect the non-constant stellar flux from other sources. The results are represented in FIG. 2. Typical M-stars large time-scale stellar variability is more obviously visible for the transit of 18 Jul, where a constant bright increase is marked, and less prominent for 20 Jul. Analyzing the relative flux during the transit, no correlated noise has been detected for the transit of 18 Jul, but it has been detected for 20 Jul. From now on, we will discuss the data from only the second transit in detail.

It is visible that the flux decreases around 0.12 days with the typical exoplanet transit shape. The stellar activity that will be studied in depth is that which occurs during transit and thus contaminates the exoatmosphere signal. Also in FIG. 2, the exoplanet transit model is fitted as well as a linear stellar activity. Further and more complex stellar models such as Gaussian Processes (GPs) were explored. However, the non-linear fit led to overfitting that eliminated the potential flare signal that takes place during the transit.

The same process was completed with H_α bandwidth. As we can deduce from FIG. 1, the signal detected in this narrow band is some orders of magnitude below the broadband one. For this reason, the statistical noise is much larger than the flux reduction produced by the exoplanet and this model could not be fitted. However, correlated noise is visible during the potential flare detected during the transit also in H_α. The maximum residual flux increasing in the correlated event is $\times 25$ larger in H_α than in the broadband. This may indicate that it is a phenomenon with H_α emission. Unlike the spots, the stellar flare hypothesis is possible since it fulfills this characteristic.

B. Stellar activity fitting

After erasing the linear stellar flux and the exoplanet transit model, we pursue to investigate the nature of the correlated noise we are studying. In FIG. 3, and FIG. 4, we used `Allesfitter` again to fit three models to the broadband flux and H_α residuals respectively. These residuals are computed directly erasing the transit and linear stellar variability model to the observed flux. Since two almost overlapped flux bumps are observed, the first guess will be one or two flares to compare with the noise generated by a possible starspot. Once the fit is completed, the 1-flare model significantly reduces the correlated noise in both bandwidths. The second flare leaves some negative residuals in the broadband and is found very faint in the H_α. Starspot fit parameters did not converge for our sample. Thus, no spot model improves the residuals from the transit. In addition to the H_α emission found and the sharp shape, everything would indicate that this stellar activity is a flare. MCMC-derived parameters values and correlations are shown in Appendix V A for the 20 Jul 2022 transit model and linear variabil-

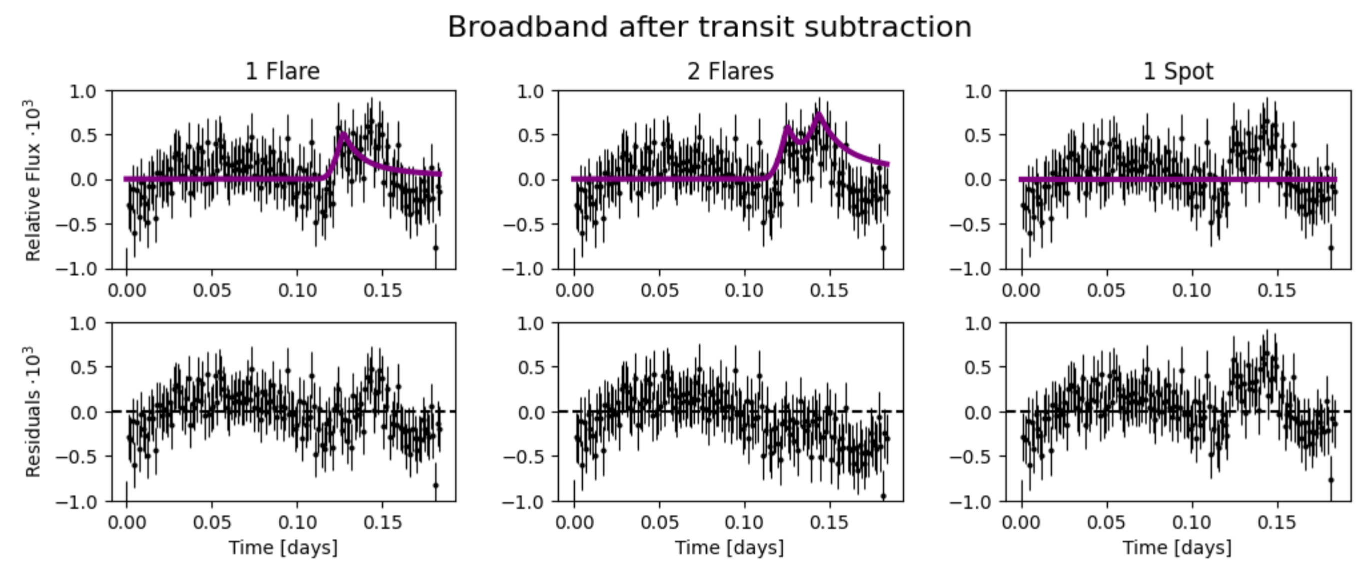

FIG. 3: Broadband relative flux residuals multiplied by 10^3 as a function of time in days. After a linear stellar activity and TRAPPIST-1 b, 20 Jul 2022, transit models extraction, the first row panels are the residuals. The curves in purple are the fits to the correlated noise observed around 0.12 days. In the second row are the new residuals after subtracting the model in the panel right above (flares or spot) and the transit and linear activity. From left to right the models suited in each column are 1-Flare, 2-Flares, and starspot. The flux errors are the standard deviation of the data points. Fits were performed with `Allesfitter`.

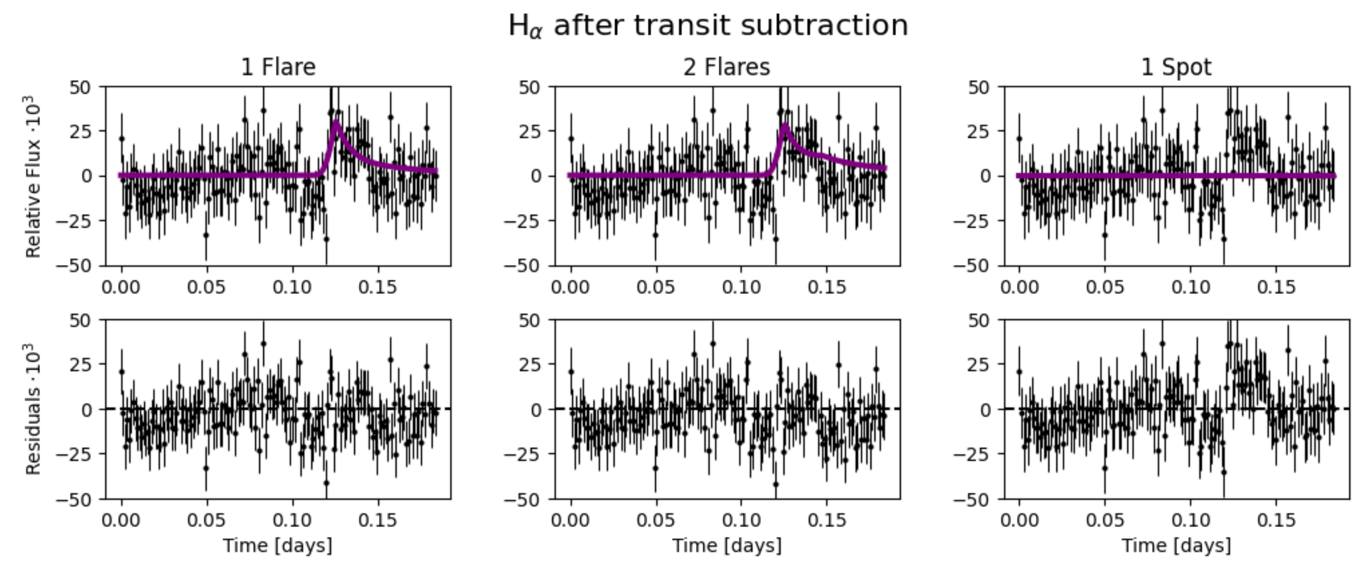

FIG. 4: H_α integration relative flux residuals multiplied by 10^3 as a function of time in days. The first row panels are the residuals after a linear stellar activity extraction. Fluxes are derived from the spectra taken during the transit of TRAPPIST-1 b, 20 Jul 2022. The curves in purple are the fits to the correlated noise observed around 0.12 days. In the second row are the new residuals after subtracting the model in the panel right above (flares or spot) and the transit and linear activity. From left to right the models suited in each column are 1-Flare, 2-Flares, and starspot. The flux errors are the standard deviation of the data points. Fits were performed with `Allesfitter`.

ity.

To compare the goodness of the fit we can use the χ^2 test. For the broadband integrated relative flux, the number of parameters fitted on the exoplanet transit and the linear star activity is 18. Every extra flare adds three parameters more and every starspot adds four. For the 1-flare model ${\chi_{1f}}^2 \approx 49.94$. For the 2-flare model, the value is ${\chi_{2f}}^2 \approx 58.59$. For the spot model, the value is ${\chi_s}^2 \approx 51.87$. The next step is to compare χ^2 for the three cases, considering the added parameters in the different models to compute the reduced value. The result is still better for the 1-flare model. The reduced values are $\chi_R^2 \approx 0.378$ for 1-flare, $\chi_R^2 \approx 0.444$ for 2-flares and $\chi_R^2 \approx 0.393$ for the spot

C. Stellar flares and exoatmospheres

One approach to illustrate the bias of flare signal over atmospheric characterization can be to compare the relative flux increased by the flare at the peak versus the typical atmospheric signal. For an exoplanet as TRAPPIST-1 b, the signature added to the relative flux by a simulated 10 bar high CO_2 atmosphere would be $\sim$20–200 ppm [10]. This range varies according to the wavelength since the flare's black body spectrum effective temperature and emission lines differ from the star's surface. The maximum value of the flare model fitted to the broadband integration in FIG. 3 is 650ppm. Thus, the signal from the flare is greater than the atmospheric absorption in the broadband. Therefore, if ignored, this stellar activity would mask the flux absorbed by the atmosphere during the transit in most wavelengths and biomarkers. Misidentifying the origin of the flare signal, e.g., treating it as a starspot, would lead to miscorrection of the flux transmitted at different wavelengths by subtracting another type of spectrum.

The implications of a flare detection during the transit are not only photometric. An event of this type may also directly interact with and affect the composition of the exoatmosphere. Many species are chemically depleted for a time by the increased UV irradiance due to the emission of the flare that provides sufficient energy to initiate certain chemical chains [11]. The equilibrium is reached again after some stellar quiescence time. Such a change is predicted to be detectable with some JWST onboard instruments for a very energetic or a recurrence of flares, adding a signal up to 1200ppm to the relative flux. At the biological level, recurrent flares of these characteristics on a planet orbiting the HZ of an M-star could be fatal to complex living organisms [12]. Nevertheless, an atmosphere depth of one-tenth of the terrestrial one could be enough to shield the consequences and event take benefit of the extra energy provided to the planet [13].

IV. CONCLUSIONS

After reducing and analyzing JWST temporal spectrometric data from two TRAPPIST-1 b transits, integrations for all the wavelengths and H_α have been performed to obtain the light curves. For the broadband of the first transit (18 Jul 2022) typical M-star large time-scale variability has been found. In the second transit (20 Jul 2022) correlated signals after erasing the transit model and linear stellar variability have been detected while the exoplanet passes in front of the star. The same sharp and time-evolving signal is $\times$ 25 enhanced in H_α. Therefore, the studied event has important emissions in the H_α. The correlated signal in active M-type stars is usually attributed to stellar flares or starspots that rotate and evolve. To keep investigating the nature of this event, we used `Allesfitter` to perform different fits to the residuals of the transit. After the χ^2 test, the 1-flare model best fits compared to the 2-flare and starspot. Together with the H_α emission, a stellar flare has become the main candidate to be the origin of the event. Identifying and correcting properly these events in every wavelength is essential because the signal added by this short-time activity may be greater than that of a hypothetical atmosphere. For instance, the temporal maximum of the flare found adds 650ppm to the relative flux versus the $\sim$ 20-200 ppm signature of a CO_2 atmosphere. A strong and repeated flare event is expected to be strongly interacting and potentially fatal to complex biological forms if the atmospheric depth is too low. More observations and theoretical work are needed to minimize stellar activity contamination in exoatmospheric transmitted spectra. In this direction, ESA's Ariel mission will have as one of its objectives to study the interaction between the host star and the planet orbiting it. It will do so by characterizing more than 1000 exoatmospheres of planets and stars of different types and its launch is planned around 2029. [14]

Acknowledgments

I would like to express my gratitude to my advisor, Octavi Fors, for always being attentive and willing to help. Many thanks to Olivia Lim and Maximilian N. Günther for assisting this desperate student. Credits to Adrià for solving my technical problems. Finally, this would have been impossible without the moral support of my parents and my roommates Rita, Ricard, and Martí who have made this alien hunting thing a bit more fun.

[1] N. Madhusudhan et al., ApJL **956**, L13 (2023).
[2] X. Bonfils et al., A&A **549**, A109 (2013).
[3] E. Agol et al., PSJ **2**, 1 (2021).
[4] O. Lim et al., ApJL **955**, L22 (2023).
[5] W. S. Howard et al., ApJ **959**, 64 (2023).
[6] M. Radica et al., MNRAS **524**, 835 (2023).
[7] M. N. Günther et al., ApJS **254**, 13 (2021).
[8] P. F. L. Maxted, A&A **591**, A111 (2016).
[9] P. C. Gregory, *Bayesian Logical Data Analysis for the Physical Sciences* (Cambridge University Press, 2005).
[10] J. Lustig-Yaeger et al., AJ **158**, 27 (2019).
[11] O. Venot et al., ApJ **830**, 77 (2016).
[12] W. S. Howard et al., ApJL **860**, L30 (2018).
[13] Y. A. Yamashiki et al., ApJ **881**, 114 (2019).
[14] G. Tinetti et al., ExpAst **46**, 135 (2018).

V. APPENDIX

A. MCMC transit parameters

Markov-Chain Monte Carlo (MCMC) is a class of methods to fit a function to describe some data. The fitted function depends on a list of parameters, that are derived simultaneously. In the case of an exoplanet transit, these parameters used have physical meaning. The final function depends on orbital values, size, inclination, and stellar limb darkening. The values encountered are shown in Table I. While fitting, correlation shapes between parameters are also derived. In Fig. 5, a correlation map between every two parameters is shown.

TABLE I: TRAPPIST-1 b transit parameters for 18 Jul 2022 using JWST NIRISS data. The values are derived using MCMC performed by `Allesfitter`.

Parameter	Value
Derived parameters	
Host radius over semi-major axis b; $R_\star/a_\mathrm{b}$	$0.0525^{+0.0040}_{-0.0035}$
Semi-major axis b over host radius; $a_\mathrm{b}/R_\star$	19.1 ± 1.4
Companion radius b over semi-major axis b; $R_\mathrm{b}/a_\mathrm{b}$	$0.00447^{+0.00048}_{-0.00039}$
Companion radius b; R_b ($\mathrm{R}_\oplus$)	1.120 ± 0.099
Companion radius b; R_b ($\mathrm{R_{jup}}$)	0.0999 ± 0.0088
Semi-major axis b; a_b ($\mathrm{R}_\odot$)	2.28 ± 0.25
Semi-major axis b; a_b (AU)	0.0106 ± 0.0011
Inclination b; i_b (deg)	$88.80^{+0.78}_{-0.54}$
Impact parameter b; $b_\mathrm{tra;b}$	$0.40^{+0.14}_{-0.25}$
Total transit duration b; $T_\mathrm{tot;b}$ (h)	$0.6104^{+0.0073}_{-0.0077}$
Full-transit duration b; $T_\mathrm{full;b}$ (h)	$0.497^{+0.013}_{-0.020}$
Host density from orbit b; $\rho_{\star;\mathrm{b}}$ (cgs)	57^{+13}_{-11}
Equilibrium temperature b; $T_\mathrm{eq;b}$ (K)	$380.^{+15}_{-13}$
Transit depth (undil.) b; $\delta_\mathrm{tr;undil;b;JWST}$ (ppt)	$8.58^{+0.11}_{-0.12}$
Transit depth (dil.) b; $\delta_\mathrm{tr;dil;b;JWST}$ (ppt)	$8.58^{+0.11}_{-0.12}$
Limb darkening; $u_\mathrm{1;JWST}$	0.48 ± 0.18
Limb darkening; $u_\mathrm{2;JWST}$	$0.12^{+0.33}_{-0.31}$
Combined host density from all orbits; $rho_{\star;\mathrm{combined}}$ (cgs)	57^{+13}_{-11}

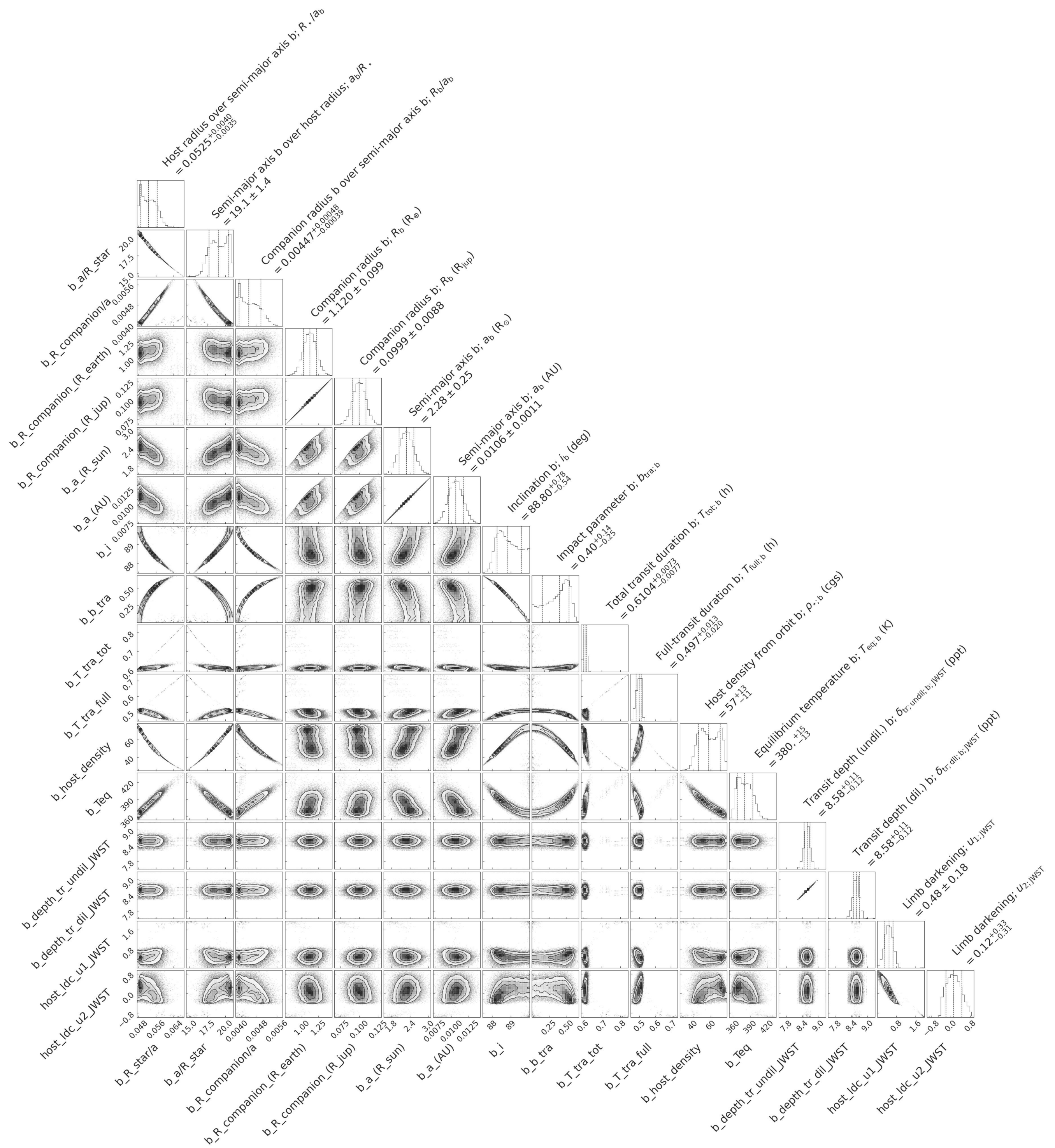

FIG. 5: MCMC correlation between transit parameters. Every plot is the correlation map between the parameter labeled under the column and at the left of the row.